

Reduced Wave Speed in 3D Printed Corrugated Pipes

Halle Theriault
The Department of Physics and Astronomy
The University of North Carolina Asheville
One University Heights
Asheville, North Carolina 28804 USA

Faculty Mentor(s):
Dr. James Perkins

Abstract

As sound waves travel through a corrugated tube, the speed of sound is reduced. This surprising but consequential phenomenon also occurs in "bumpy"--i.e., periodically perturbed--materials in the fields of electronics, solid-state physics, and optics--where, for example, it explains the refraction of light in water. Two different models can be used to explain this effect in acoustics: the Bloch periodic wave theory and the Cummings suppressed mass model. However, the two models differ in their predictions of how the speed of sound varies with corrugation depth, width, and spacing. To test these two theories, the speed of sound was measured using 3D modeled and printed corrugated tubes which allowed for precise control of the corrugation parameters. Computational finite element analysis (FEA) supported our experimental results, which suggests that the Griffiths model underpredicts and the Cummings model overpredicts the speed reduction. Experimental results from the first set of nine tubes and FEA results will be helpful in creating a third model.

1. Introduction

At typical temperature and humidity, sound travels through air at a constant speed of 343 m/s.¹ Interestingly, as sound travels through corrugated pipes, its speed is attenuated by an amount that depends on the corrugation parameters. When changes

in the radius are periodic, the speed reduction (n) is predicted by two models: the Griffiths periodic wave theory and the Cummings suppressed mass model.²

$$n = \frac{v_{eff}}{v} = \sqrt{\frac{V_{pipe}}{V_{pipe} + V_{corr}}} \approx \left(1 - \frac{wh}{sr}\right)^{-1}$$

Where v_{eff} is the speed of sound in the corrugated tube, v is the speed of sound in a straight tube, V_{pipe} is the volume of the straight tube, V_{corr} is the volume inside of the corrugations of the tube, w is the width of the corrugations, h is the depth of the corrugations, s is the periodicity of corrugations, and r is the inner radius of the tube, as seen in Figure 1.

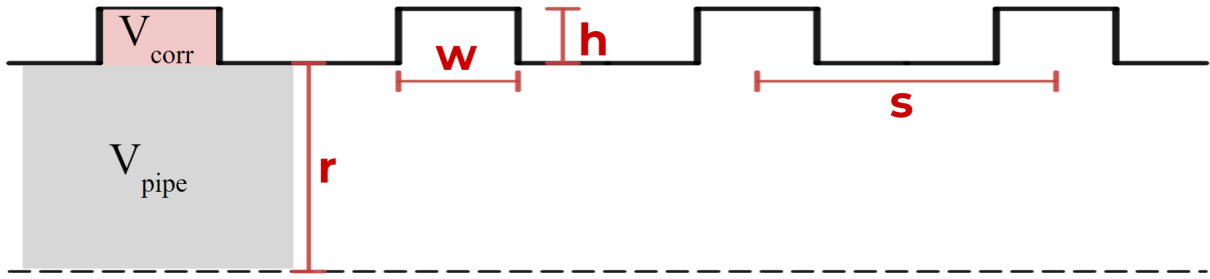


Figure 1: Cross-sectional view of the corrugated tube.

In two experimental trials, we investigated the difference between these models by measuring the speed of sound in nine 3D-printed tubes. Computational finite element analysis simulations agreed closely with experimental results, showing that the Griffiths theory underpredicts and the Cummings model overpredicts the speed reduction.

Waves in periodic media are a broadly applicable isomorphism for the study of many different types of systems, including leaky wave antennas, solid-state lattices, optical waveguides, and – as is the case in this work – corrugated tubes. Using acoustic waves in pipes is a valuable model for use in an undergraduate laboratory because the dimensions of the periodicity are on an easily fabricated, human scale; sources and detectors are commercially available, such as microphones and speakers; and the acoustic sounds allow the students to interact with the experience aurally.

2. Theory

The speed of a disturbance in a gas can be found with several methods and pleasingly results in a derivation of the wave equation.³ In a pipe of fixed radius, this wave

equation reduces to a 1-dimensional form that is only dependent on the distance down the tube, considering that the wavelength is longer than the diameter of the pipe.

$$\frac{\partial^2 \Psi}{\partial t^2} = v^2 \left(\frac{\partial^2 \Psi}{\partial x^2} \right)$$

Adding in corrugations or changing the radius results in a difficult enough problem that closed-form solutions only exist for special formulas for the radius, such as the exponential horn.⁴ To solve this problem for rectangular corrugations, two simplifying models exist which both have different origins and give similar, but not identical results.

2.1 Griffiths Model

In the Griffiths model, a Bloch-like model, we examine the problem as one of repeated identical perturbations of the wave equation solution in each of the corrugations.⁴ As the wave travels from a non-corrugated to a corrugated region, or vice versa, there will be a phase shift in the wave. The phase shift by itself would not predict a net reduction in the speed of sound, but considering the pulse of sound as a sum of many different wavelengths (Fourier theory) where each constituent wavelength has a different phase shift, there is a net reduction in the group velocity.

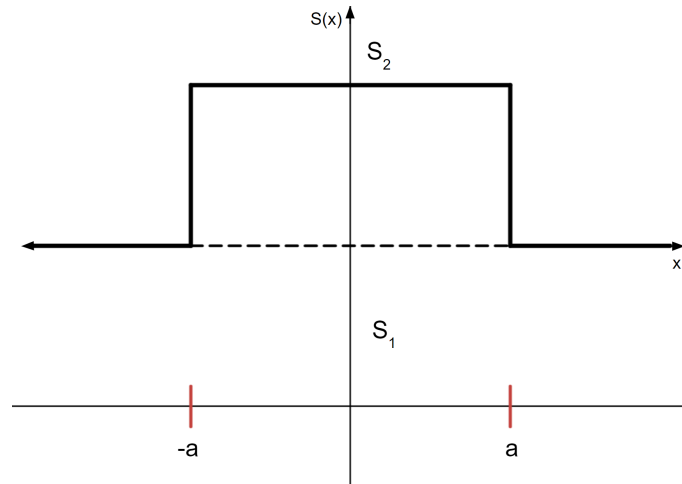


Figure 2: Cross sectional area of the rectangular corrugation, where $S(x)$ is the cross-sectional area.

The solutions in both the corrugated and non-corrugated regions of the tube are a 1-dimensional wave equation with continuous pressure at $-a$ and a , as seen in Figure 2, but its derivative is discontinuous.

$$\psi(x) = \begin{cases} Ae^{ikx} + Be^{-ikx} & \text{if } x < -a \\ Fe^{ikx} + Ge^{-ikx} & \text{if } -a < x < a \\ Ce^{ikx} + De^{-ikx} & \text{if } x > a. \end{cases}$$

The discontinuity of the pressure's spatial derivative is equal to the ratio of the cross-sectional areas, $\frac{S_1}{S_2}$. Based on this phase shift, the predicted group velocity can be predicted by following the method in Griffiths section IIIC.⁴ Solutions of this model result in non-closed-form solutions that must be found with numerical techniques.

2.2. Cummings Model

The Cummings model treats the corrugated tubes with a quasi-1-dimensional wave equation that assumes the changes to the radius, or the second dimension, are small compared to the wavelength of the sound.^{5,6} In the result of the quasi-1D equation, there exists a term that accounts for the acoustic impedance of the walls of the tube. When there are no corrugations, the impedance is zero, and the 1D-wave equation is returned. Inside the corrugations, the walls are approximated to act as a Helmholtz resonator, which has a “springy” nature and a resonance frequency that is determined by the surface area and volume of the cavity. This results in a different wave relation – or the relationship between the speed, wave number, and frequency of a wave – in the corrugated regions of the tube. Thus, the speed is reduced in these areas.⁵

3. Experimental

Along with the theoretical models of sound wave propagation inside of corrugated tubes, we 3D modeled and printed several corrugated tubes of constant inner radius, but varying other corrugation parameters such as the corrugation width, depth, and the periodicity of the corrugations.

3.1 3D Modeling

3D models of the corrugated tubes were created in Autodesk Fusion 360, a computer-aided design (CAD) program that allowed for precise control of the corrugation parameters. Parametric equation tools also allowed us to model different shapes of corrugations.

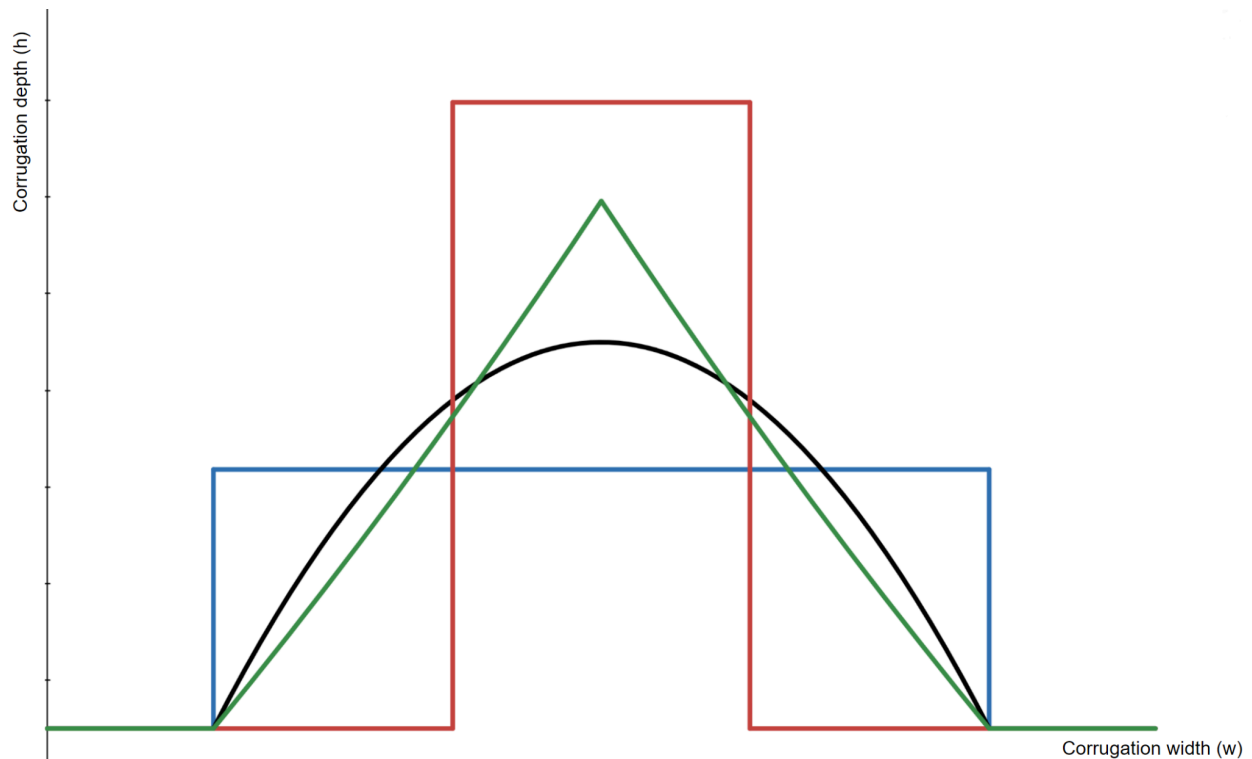


Figure 3: Different corrugation shapes that have been modeled: rectangular corrugations in red and blue, exponential (triangular) corrugations in green, and cosine (semicircle) corrugations in black.

In Figure 3 above, those specific corrugation parameters were chosen with one another because they resulted in the same speed of sound reduction according to the Cummings model, but with different corrugation shapes, widths, and depths.

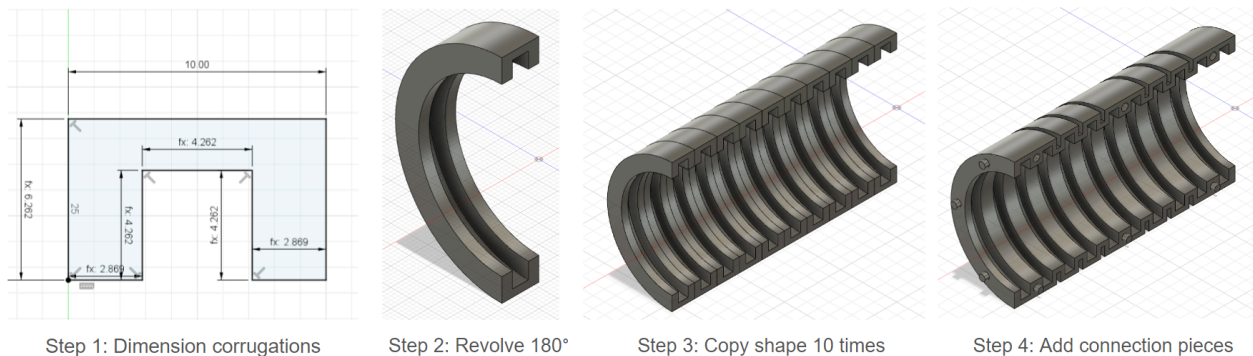


Figure 4: Steps to create a corrugated tube in Fusion 360.

Parameterizing the different corrugation dimensions with Fusion 360 allowed for quick and easy modeling of several different corrugation sizes. The step-by-step process of creating these 3D modeled tubes is illustrated in Figure 4.

3.2 3D Printing

To 3D print the CAD models of the corrugated tubes, we used the Elegoo Mars 2 Pro, an LCD resin printer, seen in Figure 5. It produces high-resolution prints that are extremely accurate – measured to be within $\pm 0.05\text{mm}$ – which is crucial for experimental data collection.



Figure 5: Elegoo Mars 2 Pro after printing tubes.

Many other parameters that are controlled by the resin printer, such as the layer height, exposure time, lifting distance, and lifting speed are all very important factors to consider when printing the tubes. Small adjustments in these parameters can cause a print to fail, wasting time and materials.

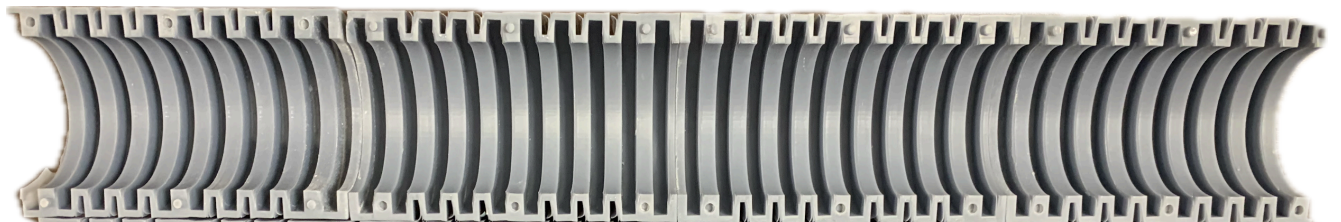


Figure 6: Picture of the cross-section of a full-length corrugated tube.

Due to the constraints of the 3D printer's build plate, which is only 120mm by 68mm, the tubes had to be printed in segments that are $\frac{1}{4}$ of the length of the full-sized tube. To

make the post-printing process easier, the tubes were also printed in halves, where each full-sized tube consisted of eight segments. A group of four segments takes about 10 hours, so each tube takes about 20 hours of print time alone. The segments were connected by their alignment pieces and caulk was used on the seams to create an air-tight seal. A cross-section of four out of the eight 3D printed segments is illustrated in Figure 6.

3.3 Experimental Procedure

After printing the different series of corrugated tubes, we used the experimental setup seen in Figure 7 following Klomp *et al.* that allowed us to take a time-of-flight measurement of the sound inside of the tube.⁵

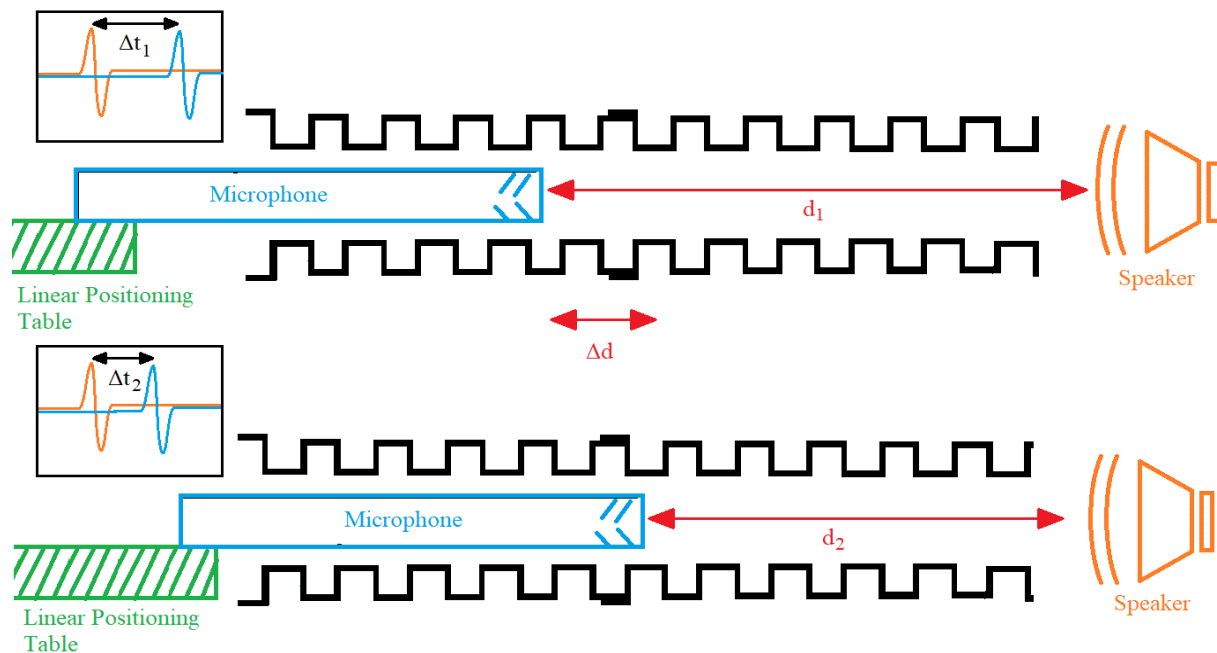


Figure 7: Diagram of the experimental setup.

The time that it takes the sound to travel from the speaker to the microphone inside of the tube is measured at several different equally-spaced microphone distances. Graphs of the measurements taken with the microphone furthest away from the speaker and closest to the speaker are seen in Figure 8.

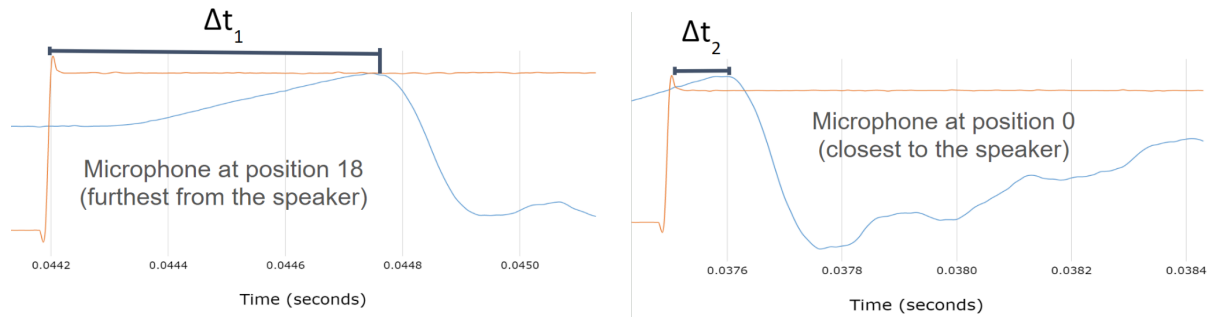


Figure 8: Detector signal at two different microphone positions.

The slope of the plot of the microphone distance vs the time delay between the control signal and detection gives the speed of sound. An example of this is illustrated in Figure 9.

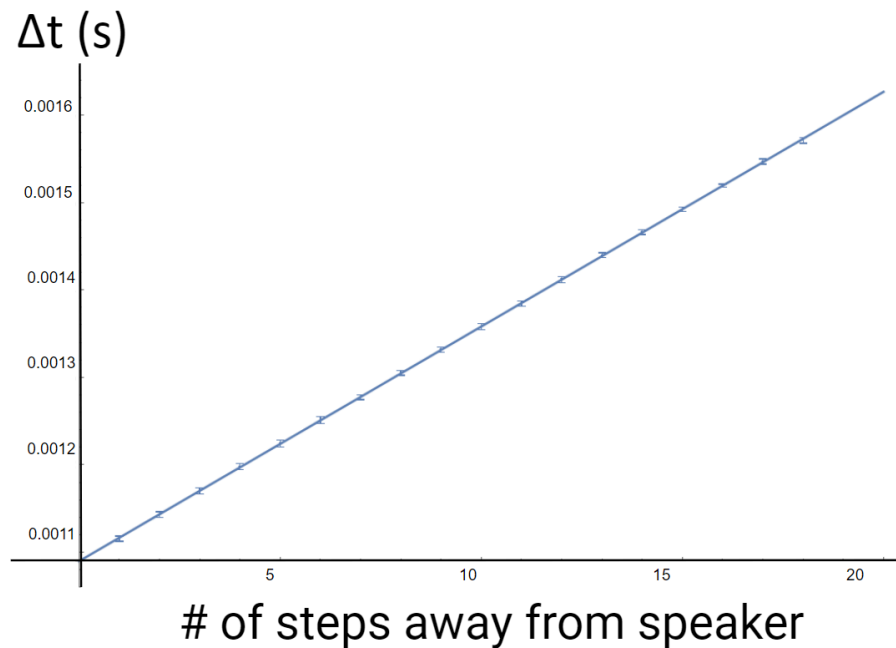


Figure 9: Graph of the speed of sound measurement as a function of steps away from the speaker vs. change in time.

We measured the speed of sound through a straight Boomwhacker acting as our control tube. Since this tube doesn't have any corrugations, we can adjust the other measurements we take based on the expected value from the straight tube. The speed reduction coefficient should be 1, so the difference in the measured speed reduction with the Boomwhacker and the predicted speed reduction is taken into account when analyzing the measured data from the nine corrugated tubes.

To automate the data collection process, we used LabVIEW, a visual programming language useful for instrument control and data collection.

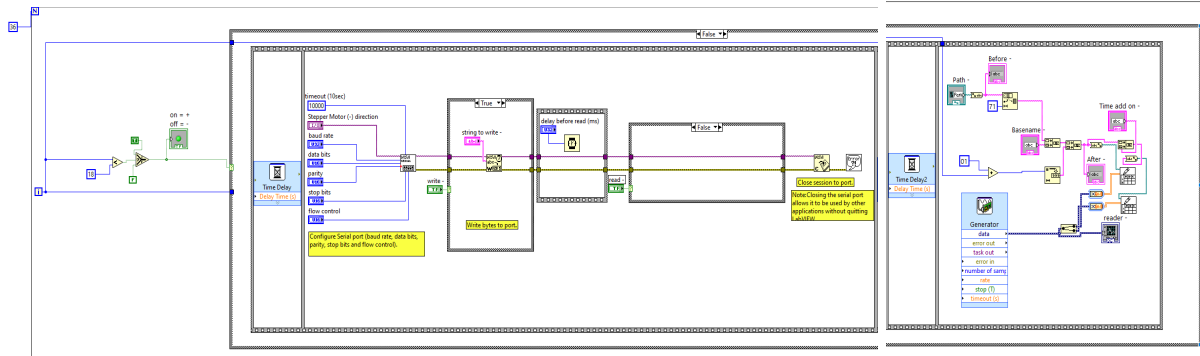


Figure 10: LabVIEW block diagram.

Creating nested loops inside LabVIEW, seen in Figure 10, allowed us to collect all of the data for one tube in as little as three minutes, which is $\frac{1}{5}$ of the time it took to collect the same amount of data before automating the process. The linear translation movement of the microphone was programmed and the data collected from the microphone was automatically exported to a spreadsheet. We collected five series of data points for each microphone position, shown in Figure 11, and ran two separate measurements of each tube, resulting in 180 data points for each tube.

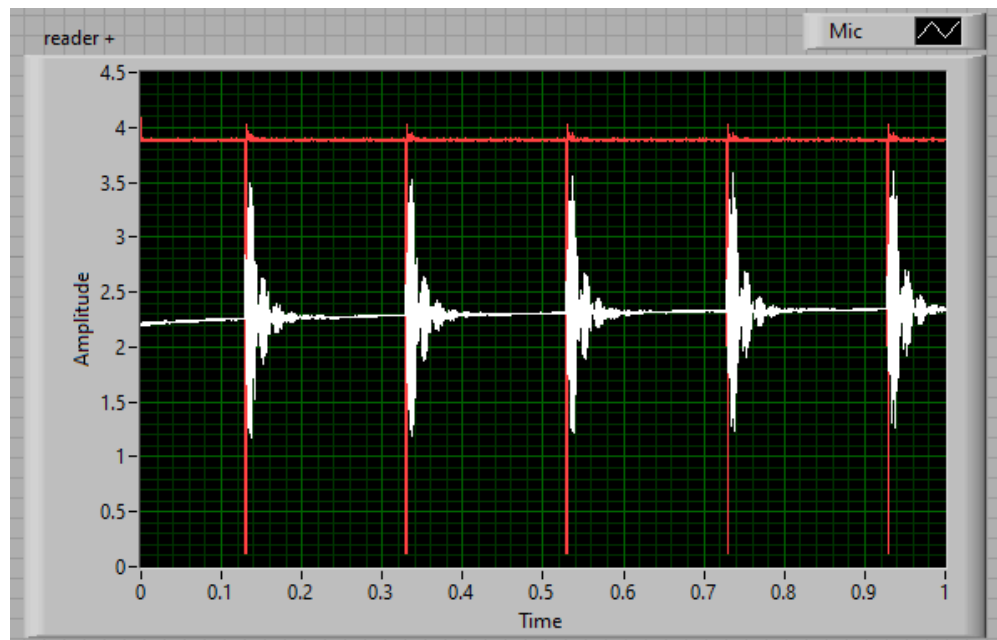


Figure 11: Output reader from the speaker (in red) and the microphone (in white).

3.5 Finite Element Analysis

While this work focuses on theoretical predictions and experimental results, a separate colleague also performed a finite element analysis (FEA) using Ansys on the internal volume of each tube. In FEA, the region of the gas is broken up into small volumes over which it is possible to approximate time-dependent solutions to the wave equation, illustrated in Figure 12. This numerical technique gives another approximation to the result we're seeking.

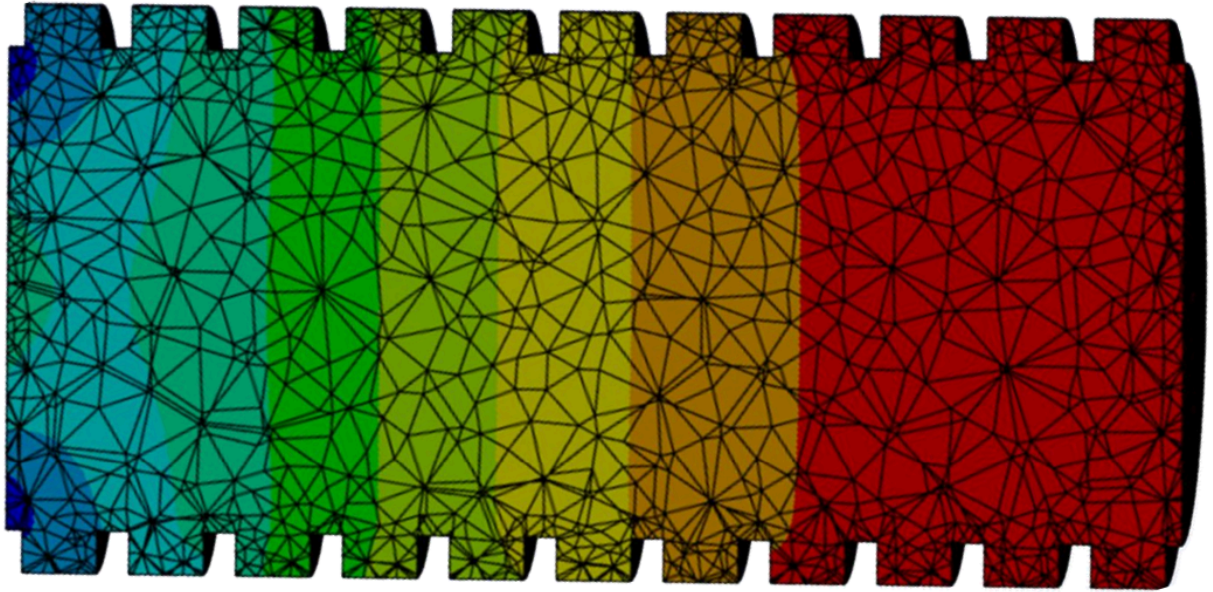


Figure 12: Cross section of the volume inside of a corrugated tube.

Future co-authored publications will have more information on the FEA, but it is included here because of how well it agrees with the experimental data--the focus of this paper.⁶

5. Results

Speeds of sounds for all nine rectangularly corrugated tubes, one cosine, one exponential, and the control tube of constant radius were measured two times and the trials can be compared in Figure 13. The only difference in the two trials was the frequency of the pulse sent down the tube (1 kHz in Experiment 1, 2 kHz in Experiment 2). While there was great agreement between the two trials, the data suggests that our statistical method is underestimating the uncertainty in measurements, but is on the right order of magnitude.

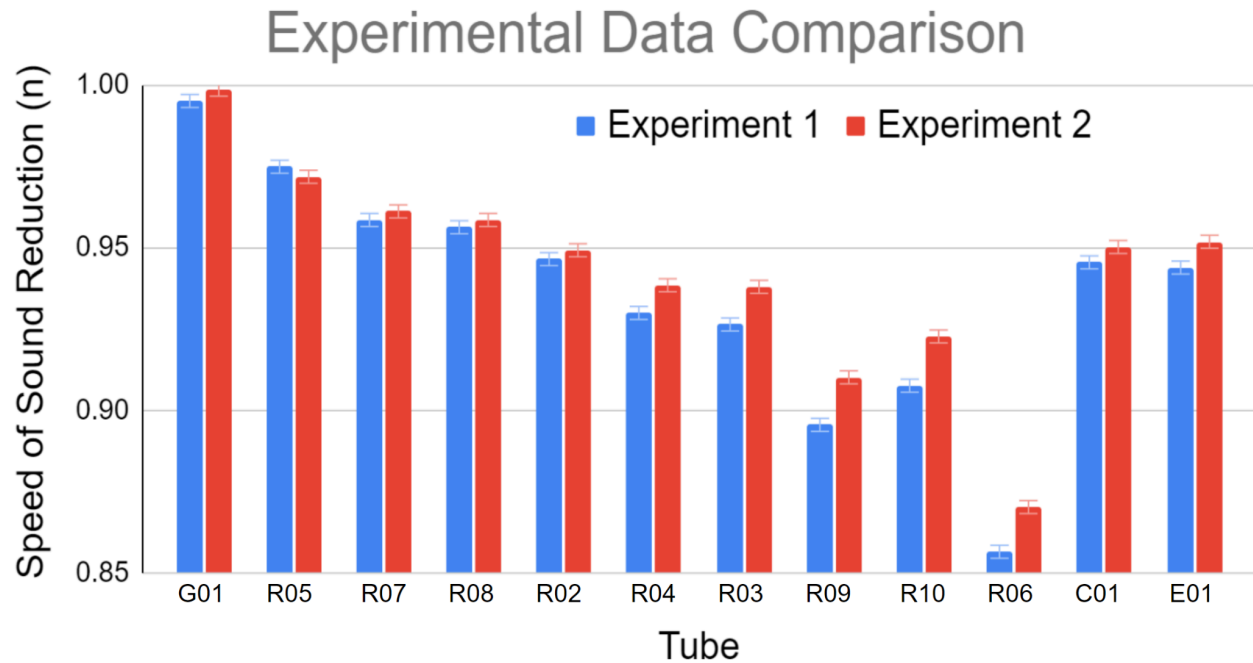


Figure 13: Two separate experimental trials taken months apart.

R02, R03, R04, C01, and E01 all have the same predicted speed of sound reduction according to the Cummings model.

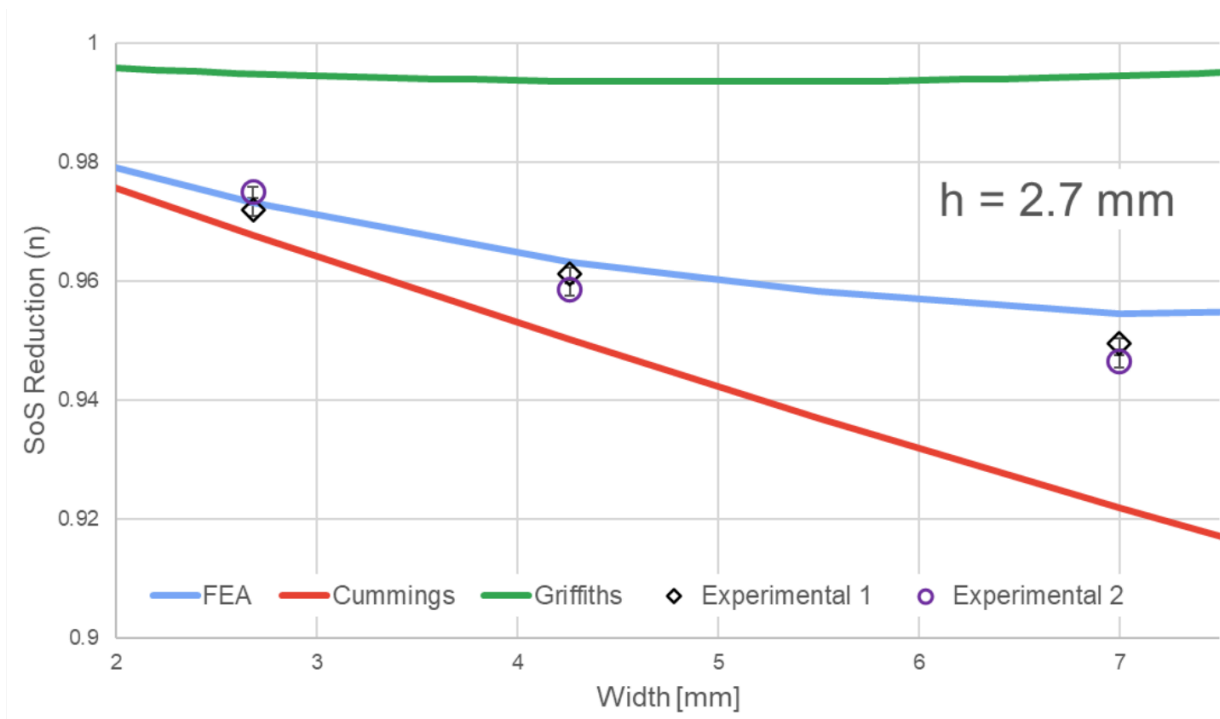


Figure 14: Analyzed results of corrugation depth 2.7mm with varying corrugation widths.

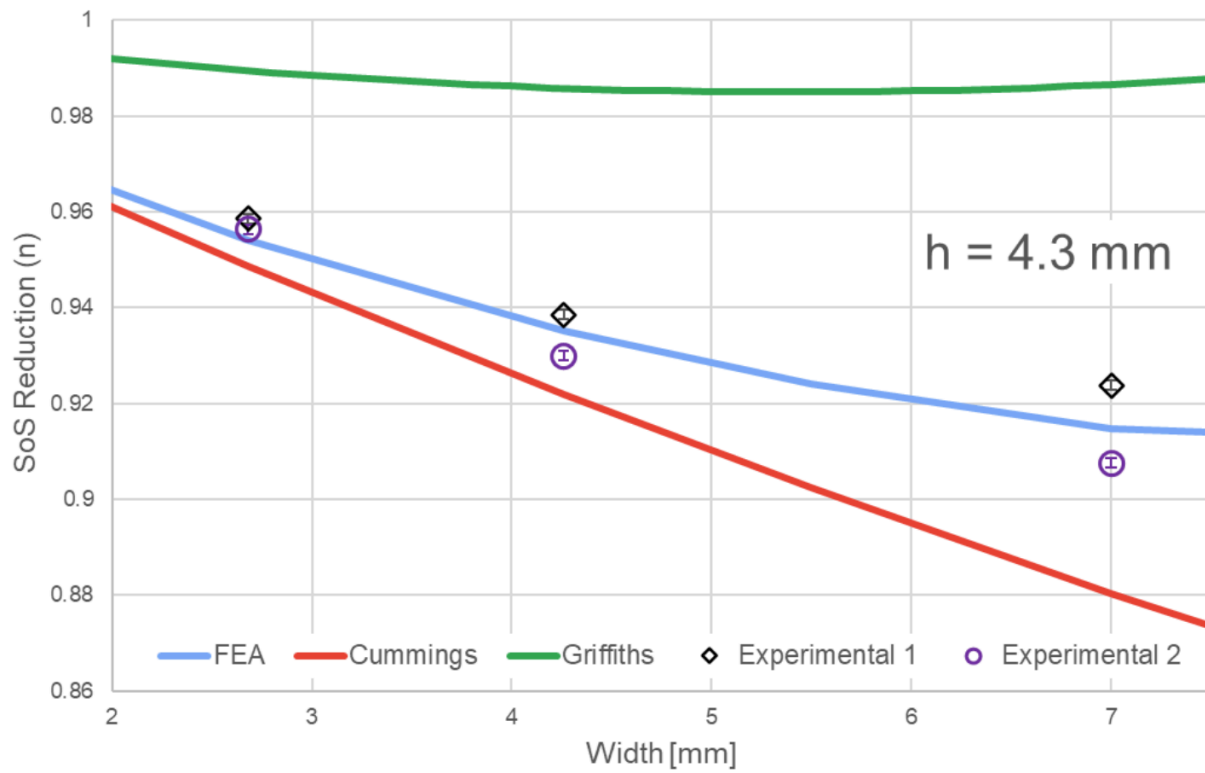


Figure 15: Analyzed results of corrugation depth 4.3mm with varying corrugation widths.

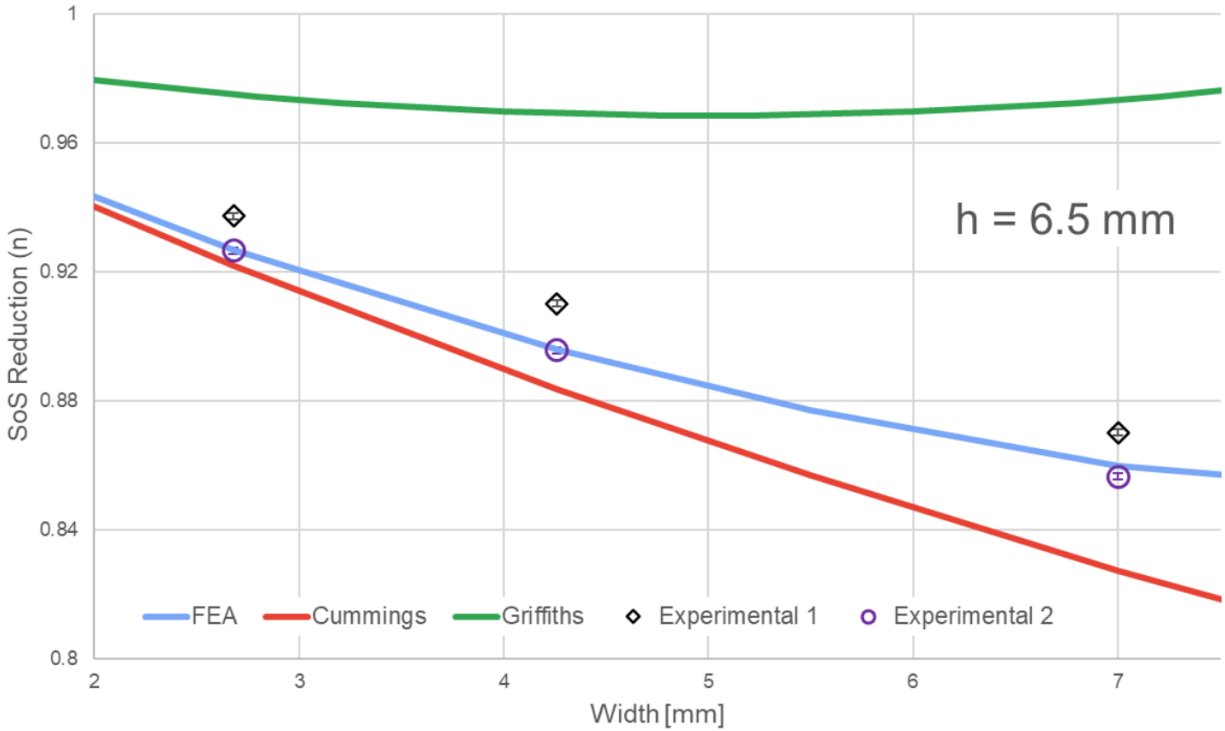


Figure 16: Analyzed results of corrugation depth 6.5mm with varying corrugation widths.

Figures 14, 15, and 16 show the speed of sound reduction vs corrugation width for three different series of tubes with corrugation depth $h = 2.7$ mm, 4.3 mm, and 6.5 mm. In general, the experimental results were best predicted by the FEA results while the Cummings model overpredicted- and the Griffiths model underpredicted the speed attenuation.

The results from FEA and the experimental data show a non-linear dependence on corrugation width, which does not agree with the Cummings model. The error bars for the experimental data are within the size of the graphics and illustrate the precision of the data collection process. Our error in the speed of sound measurement is within $(3/10)$ of a meter per second, which translates to a speed reduction error $\pm(1/1000)$.

As the width approaches the constant value of $s = 10$ mm, the length of the period, the Griffiths predicts an increasing speed of sound, while the Cummings model appears to continue to decrease approximately linearly

6. Conclusion

The speed of sound inside 10 different corrugated tubes was measured with great accuracy. The experimental results fall in between the two leading models that predict the reduction in the speed of sound but can be replicated with FEA numerical approximation. A hybrid model combining these two is suggested by this data. If a theoretical model agrees well with FEA results, it will likely compare favorably with experimental results.

7. Acknowledgments

Thank you to our research advisor, Dr. James Perkins, to the UNC Asheville Undergraduate Research Program, the UNC Asheville Department of Physics and Astronomy, my research colleagues, Quinn Foti, Alexandra Lee, and Professor Emeritus Dr. Michael J. Ruiz.

8. References

¹US Department of Commerce, N. (2023) Speed of sound calculator, Speed of Sound Calculator. Available at: https://www.weather.gov/epz/wxcalc_speedofsound.

²Ruiz, M.J. and Perkins, J. (2017) 'The Monster Sound Pipe', *Physics Education*, 52(2), p. 025002. doi:10.1088/1361-6552/52/2/025002.

³The Feynman lectures on Physics vol. I ch. 47: Sound. the wave equation. Available at: https://www.feynmanlectures.caltech.edu/I_47.html.

⁴Griffiths, D.J. and Steinke, C.A. (2001) 'Waves in locally periodic media', *American Journal of Physics*, 69(2), pp. 137–154. doi:10.1119/1.1308266.

⁵Sidebottom, D.L. (2020) 'Slow sound: An undergraduate lab experience for critical thinking', *American Journal of Physics*, 88(7), pp. 521–525. doi:10.1119/10.0001023.

⁶Elliott, J.W. (2004) in M. Wright (ed.) *Lecture notes on the Mathematics of Acoustics*. Covent Garden, London: Imperial College Press, pp. 207–222.

⁷Klomp, J., Schmit, N.U. and Sidebottom, D.L. (2021) 'The speed of sound in monster sound tubes', *Physics Education*, 56(4), p. 043009. doi:10.1088/1361-6552/abfd41.

⁸Foti, Q. (2022) 2022FallSymposium, Finite Element Analysis of Pipes with Periodically Varying Radii. Available at: <https://2022fallsymposium.sched.com/event/1EPZi/finite-element-analysis-of-pipes-with-periodically-varying-radii>.